Title

Solving the “Magic Angle” Challenge in Determining Molecular Orientation Heterogeneity at Interfaces

Journal

The Journal of Physical Chemistry C, 120(36)

ISSN

1932-7447

Authors

Li, Zhiguo
Wang, Jiaxi
Li, Yingmin
et al.

Publication Date

2016-09-15

DOI

10.1021/acs.jpcc.6b08093

Peer reviewed

Solving the "Magic Angle" Challenge in Determining Molecular Orientation Heterogeneity at Interfaces

Zhiguo Li,[1†] Jiaxi Wang,[1†] Yingmin Li,[2] Wei Xiong[*1,2]*

[1]Department of Chemistry and Biochemistry, University of California, San Diego, La Jolla, California 92093, United States

[2]Material Science and Engineering Program, University of California, San Diego, La Jolla, California 92093, United States

[†] These two authors contributed equally.

*Corresponding author. Email: w2xiong@ucsd.edu. Phone: 858-534-0270

ABSTRACT

It is critical to determine conformations of molecular monolayers in order to understand and control their functions and properties, such as efficiencies of self-assembly-based biosensors and turnover frequency of surface-bound electrocatalysts. However, surface molecules of the monolayers can adopt conformations with many different orientations. Thus, it is necessary to describe the orientations of surface molecular monolayers using both mean tilt angle and orientational distribution, which together we refer as orientation heterogeneity. Orientation heterogeneity is difficult to measure. In most cases, in order to calculate the mean tilt angle, it is assumed that the orientational distribution is narrow. This assumption causes ambiguities in determining the mean tilt angle, and loss of orientational distribution information, which is known as the "magic angle" challenge. Using heterodyne two-dimensional vibrational sum frequency generation (HD 2D VSFG) spectroscopy, we report a novel method to solve the "magic angle" challenge, by simultaneously measuring mean tilt angle and orientational distribution of molecular monolayers. We applied this new method to a CO_2 reduction catalyst/gold interface and found that the catalysts formed a monolayer with a mean tilt angle between its quasi-C_3 symmetric axis and the surface normal of 53°, with 5° orientational distribution. The narrow orientational distribution indicates that the surface molecules are rigid, which sample only limited configurations for facilitating a reaction, because of the short anchoring groups. Although applied to a specific system, this method is a general way to determine the orientation heterogeneity of an ensemble-averaged molecular interface.

1. INTRODUCTION

Molecular orientation at complex interfaces, including heterogeneous catalysts,[1–3] energy materials[4] and biological membranes,[5,6] is often heterogeneous. The surface molecules can form an ordered monolayer with all molecules tilted at the same angle, monolayers with randomly orientated molecules, or monolayers with complicated orientational distributions. Understanding the complex molecular orientation at these interfaces is critical to reveal the surface structure-function relationships. For example, when enzymes, such as hydrogenase and glucose oxidase, are immobilized onto electrodes to form surface electrocatalysts, it is critical to control their orientations and the corresponding distributions, in order to optimize their charge transfer rate and the mass transportation of reactants and products, for the best activities.[7] Another example is that in biological lipid membranes, lipids adopt new orientations when antimicrobial peptides intrude into the lipid membranes. Measuring the change of lipid orientation can elucidate the microscopic pictures of how the membrane morphologies respond to the invading peptides, which could have important implications for drug designs.[6]

To describe the molecular orientation of monolayers, a Gaussian distribution is a common model to use. More complex orientational distribution model could exist, but the Gaussian distribution model provides a basic description of the orientation heterogeneity of the molecular monolayers. In the Gaussian distribution model, two physical quantities need to be measured – the mean tilt angle θ_0 and the orientational distribution σ, which we refer to as the (θ_0, σ) pair or orientation heterogeneity hereafter.

It is a challenge to measure orientation heterogeneity. For decades, surface-specific vibrational sum frequency generation spectroscopy (referred to as 1D VSFG hereafter)[8–16] has

been used to determine the mean tilt angle, under the assumption of a narrow orientational distribution. However, in this case, the knowledge of orientational distribution is lost, and the measured mean tilt angle can deviate from the real mean tilt angle when the orientational distribution is large, which is the well-known "magic angle" challenge.

This issue arises from that 1D VSFG measures an orientation parameter D_1 that is equal to

$$D_1 = \frac{\langle \cos^3\theta \rangle}{\langle \cos\theta \rangle} = \frac{\int_0^{\pi} \cos^3\theta \cdot G(\theta;\ \theta_0,\ \sigma) d\theta}{\int_0^{\pi} \cos\theta \cdot G(\theta;\ \theta_0,\ \sigma) d\theta} \quad (1)$$

where θ is the angle between the surface normal and the molecular axis, and the bracket means orientational average (integrating the products of cosine functions and a modified Gaussian distribution $G(\theta;\theta_0, \sigma)$ from 0° to 180°).[17–21] Clearly, D_1 is a function of the (θ_0, σ) pair, so a single D_1 cannot warrant a unique solution to both θ_0 and σ.

When the orientational distribution is assumed to be narrow (σ=0°), D_1 can be simplified to $\cos^2\theta_0$, and the mean tilt angle (θ_0) can be calculated. While it works fine for well-ordered, self-assembled monolayers, for most molecular monolayers, this narrow angular distribution assumption is not always valid.[22] In the broad angular distribution case, each D_1 corresponds to many pairs of (θ_0, σ) (solid lines in Figure 1a). For instance, if D_1=0.600 is measured, the net orientation can either be θ_0 =39.2° with a uniform distribution (σ=0°) or any other mean tilt angle with a broad distribution (σ=90°) (Figure 1b). This 39.2°, referred to as the "magic angle", represents the extreme case of ambiguities in determining orientation heterogeneity,[22] while similar ambiguity also remains for any other D_1 values. In summary, the "magic angle" challenge results in two areas of uncertainty in determining orientation heterogeneity: first, the mean tilt

angle measurement can be inaccurate, and second, the orientational distribution is unknown. Although this challenge has been well-known for more than a decade,[22–25] no general solutions to it have been proposed, to the best of our knowledge.

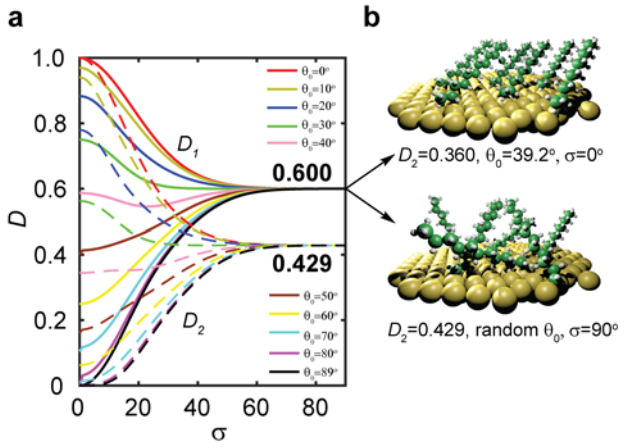

Figure 1. The "magic angle" challenge in determining molecular orientation and its solution by using a combination of D_1 and D_2. (a) Orientational parameters D_1 (solid line) and D_2 (dashed line) as a function of orientational distribution θ_0 for a series of mean tilt angles θ_0. D_1 and D_2 are calculated based on a modified Gaussian function.[22] Details about this function are described in the supporting information. (b) When only D_1=0.600 is measured, it is unknown whether the surface has a uniform orientation distribution with θ_0=39.2° or a broad orientation distribution. However, the D_2 is different for these two scenarios.

To determine the orientation heterogeneity, another independent quantity besides D_1 needs to be measured, often by using a second spectroscopy. For instance, by combining second harmonic generation (SHG) and another linear spectroscopic method, such as angle-resolved absorbance[21], linear reflection[26,27], or polarization-resolved fluorescence detection[28–31], the orientational distribution of molecules in thin films can be determined. These methods all rely on spectroscopies that are not intrinsically surface-sensitive and, therefore, have been mainly used

to study thin film samples. There have been a few attempts to determine interfacial molecular orientation using non-linear optical methods. Eisenthal and co-workers modified the polarization-resolved SHG by adding a circularly polarized pump pulse. The pump pulse created a non-equilibrium population of surface molecules, which was used to determine the orientational distribution.[32] Also, by taking measurements at various beam incidence angles and carefully calculating parameters related to experimental setup, Wang and co-workers showed that it is possible to extract the molecular orientational distribution from the SHG measurements.[33]

In this work, using surface sensitive heterodyne two dimensional vibrational sum frequency generation (HD 2D VSFG) spectroscopy, we introduce a novel and general method to determine orientation heterogeneity and solve the "magic angle" challenge for surface science, based on a single measurement. In particular, we studied a surface catalytic system for CO_2 reduction as well as solar energy applications. The molecular structure and dynamics of this catalytic system have been investigated extensively with various spectroscopic methods,[34–38] but its surface molecular orientation heterogeneity has yet to be revealed, which is a critical step to better understand the surface structure-function relationship. By measuring the orientation heterogeneity with no general assumptions, we learned that the surface catalysts form a rigid, ordered monolayer, which could influence the conformational evolution of catalysts in a catalytic cycle. This information that is unavailable previously can shed new insight to the structure-function relationship and have new implications for rationale designs of surface catalysts.

2. THEORETICAL FRAMEWORK OF ORIENTATIONAL ANALYSIS

2.1 Measuring Orientation Heterogeneity using HD 2D VSFG. To determine surface molecular orientation heterogeneity, the key is to measure a second independent orientation parameter along with D_1. We used HD 2D VSFG to determine the second orientation parameter $D_2=\langle\cos^5\theta\rangle/\langle\cos\theta\rangle$. Since D_1 and D_2 have different dependence on θ_0 and σ (Figure 1a), a unique pair of θ_0 and σ can be determined.

The recently developed HD 2D VSFG spectroscopy[39–43] is the core measurement that enables surface molecular orientation heterogeneity characterization. The experimental detail of this spectroscopic technique will be described in section 3. Overall, fourth-order susceptibilities ($\chi^{(4)}_{eff}$) are measured in HD 2D VSFG. Similar to 1D VSFG, which measures second-order susceptibilities ($\chi^{(2)}_{eff}$), these even-order nonlinear optical signals only survive in non-centrosymmetric environments, such as interfaces. Therefore, both 1D and HD 2D VSFG spectroscopies are interface-specific vibrational spectroscopies whose signals depend on the molecular orientations.[10,17,42,44]

The key relationship that enables HD 2D VSFG spectroscopy to measure surface molecular orientation heterogeneity is that $\chi^{(2)}_{eff}$ and $\chi^{(4)}_{eff}$ can be expressed as a linear combination of $\langle\cos\theta\rangle$, $\langle\cos^3\theta\rangle$ and $\langle\cos^5\theta\rangle$ (Eq. 2).

$$\chi^{(2)}_{eff,i} = a_i\left\langle\cos\theta\right\rangle + b_i\left\langle\cos^3\theta\right\rangle$$
$$\chi^{(4)}_{eff,i} = c_i\left\langle\cos\theta\right\rangle + d_i\left\langle\cos^3\theta\right\rangle + e_i\left\langle\cos^5\theta\right\rangle \quad (2)$$

These equations resulted from a series of Euler transformations to convert molecular frame hyperpolarizabilities to lab frame susceptibilities, where a_i, b_i, c_i, d_i and e_i are constants that depend on the molecular hyperpolarizabilities of the i^{th} vibrational mode (supporting information

for details). Since heterodyne 1D VSFG is simultaneously measured as heterodyne 2D VSFG is taken, both $\chi^{(2)}_{eff}$ *and* $\chi^{(4)}_{eff}$ can be determined from the same HD 2D VSFG experiments.

By taking the ratios of χ_{eff} between two vibrational modes,[45] or ratios of χ_{eff} of a single vibrational mode under different polarization combinations,[17] we obtain the key formula (Eq. 3) to extract D_1, D_2 from $\chi^{(2)}_{eff}$ and $\chi^{(4)}_{eff}$:

$$\frac{\chi^{(2)}_{eff,1}}{\chi^{(2)}_{eff,2}} = \frac{a_1 + b_1 \langle \cos^3\theta \rangle / \langle \cos\theta \rangle}{a_2 + b_2 \langle \cos^3\theta \rangle / \langle \cos\theta \rangle} = \frac{a_1 + b_1 \cdot D_1}{a_2 + b_2 \cdot D_1}$$
$$\frac{\chi^{(4)}_{eff,1}}{\chi^{(4)}_{eff,2}} = \frac{c_1 + d_1 \cdot \langle \cos^3\theta \rangle / \langle \cos\theta \rangle + e_1 \cdot \langle \cos^5\theta \rangle / \langle \cos\theta \rangle}{c_2 + d_2 \cdot \langle \cos^3\theta \rangle / \langle \cos\theta \rangle + e_1 \cdot \langle \cos^5\theta \rangle / \langle \cos\theta \rangle} = \frac{c_1 + d_1 \cdot D_1 + e_1 \cdot D_2}{c_2 + d_2 \cdot D_1 + e_2 \cdot D_2} \quad (3)$$

D_1 and D_2 have different dependence on θ_0 and σ, which is why θ_0 and σ can be solved from Ds. The dependence of D_1 and D_2 on θ_0 and σ is summarized as 3D surface plots (Figure 2), which we will use to demonstrate the graphic solution for searching (θ_0, σ) pairs below. The D-θ_0-σ surface plot can be roughly divided into two regions: region I with $\sigma \leq 40°$ and region II with $\sigma > 40°$. In region I, because of the unique values of D_1 and D_2, the (θ_0, σ) pair can be unambiguously determined. In region II, D_1 and D_2 converge to 0.600 and 0.429 asymptotically, which makes them lose the one-to-one correlation with the (θ_0, σ) pair. Although the (θ_0, σ) pair cannot be uniquely determined in region II, the two asymptotic numbers (D_1=0.600 and D_2=0.429) are unique signatures for broad orientational distribution. For instance, one important consequence of this asymptotic pair is solving the above-mentioned ambiguity of the "magic angle". When D_1 and D_2 are both measured, if the interfacial molecules all tilt at 39.2° with a narrow distribution, then D_1 should be 0.600 and D_2 should be 0.360 (when σ=0°, $D_2=D_1^2$); otherwise, with a broad angular distribution, D_1 and D_2 should be close to 0.600 and 0.429,

respectively (Figure 1b). Therefore, the orientation disorder can be determined, and there is no "magic angle" ambiguity when D_1 and D_2 are measured together.

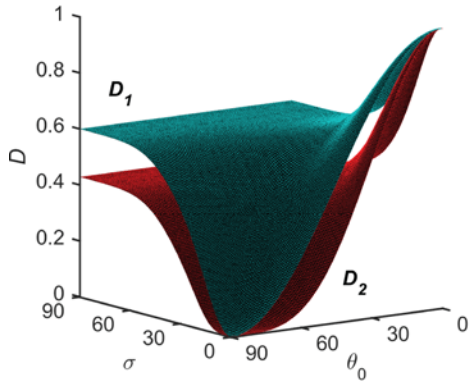

Figure 2. 3D surface of D_1 and D_2 as a function of mean tilt angle θ_0 and orientational distribution σ. D_1 is plotted in blue and D_2 in red. The projection of these surfaces on the D-σ plane is equivalent to Figure 1a.

2.2 Calculation of molecular hyperpolarizability using Gaussian 09. The values of hyperpolarizabilities determines the coefficient in Eq. 2 and 3, and the molecular hyperpolarizability tensor elements for A'(1) and A'(2) modes are determined based on the following equation:[46]

$$\beta_{ijk}^{q} \propto \frac{1}{\omega_q} \cdot \frac{\partial \alpha_{ij}}{\partial Q_q} \cdot \frac{\partial \mu_k}{\partial Q_q}$$

$$\beta_{ijklm}^{q} \propto \frac{1}{\omega_q^3} \cdot \frac{\partial \alpha_{ij}}{\partial Q_q} \cdot \frac{\partial \mu_k}{\partial Q_q} \cdot \frac{\partial \mu_l}{\partial Q_q} \cdot \frac{\partial \mu_m}{\partial Q_q} \qquad (4)$$

where $i, j, k, l, m = x, y, z$; ω_q and Q_q are the vibrational frequency and the normal coordinates of the q^{th} vibrational mode.

To determine the value of hyperpolarizability, we implement high level DFT calculations. Energy and geometry optimization of Re-complex molecule were performed using B3LYP functional and LANL2TZ basis set with Gaussian 09. Dipole derivatives ($\partial\mu/\partial Q_q$) and polarizability derivatives ($\partial\alpha/\partial Q_q$) of each vibrational mode were obtained using the keyword "polar" and "iop(7/33=1)". We calculated the hyperpolarizability and depolarization ratio using the following functional and basis set combinations: B3LYP/LanL2TZ, B3LYP/Def2QZVP, B3LYP/Def2TZVP, M06L/LanL2TZ, M06L/Def2QZVP and M06L/Def2TZVP. In orientational analysis, we used the values calculated from B3LYP/LanL2TZ, which have the best agreement with the experimental measured depolarization ratios.

3. EXPERIMENTAL SECTION

3.1 HD 2D SFG spectroscopy. The detailed description of HD 2D VSFG spectroscopy can be found in our previous publication.[47] Briefly, HD 2D SFG spectrum is collected in pump-probe geometry, with additional narrow band (fwhm~1.5nm) 800nm pulse for the SFG process. Three mid-IR pulses are sent to interact with the molecular sample, where two vibrational coherences are created during t_1 and t_3 period, and the picosecond 800nm pulse is used to interact with the second vibrational coherence for sum frequency generation process (Figure 3a). During the mid-IR pulse interactions, two vibrational coherences are generated during t_1 and t_3 periods, respectively. The first coherence is measured by scanning the t_1 time from 0 to 2500 fs in steps of 20 fs using the pulse shaper (PhaseTech), where a rotating frame at f_0=1583 cm^{-1} is used to shift the oscillation period to 80 fs, so that the scanning step can meet with the Nyquist frequency requirement. To remove scatter and 1D SFG signal, instead of taking the difference between pump on and off SFG spectra, the difference SFG spectra at the same t_1 but with different pump

pulse phase are recorded, which is known as phase cycling.[48] The second vibrational coherence is upconverted to a virtue state by a picosecond 800 nm pulse and subsequently emits visible signals through sum frequency generation process. Since the 800 nm serves as a window function, the t_3 time delay are simultaneously covered by the upconversion process and the 800 nm pulse duration determines how long t_3 is "scanned". The SFG signals are heterodyned by the local oscillator from non-resonance signal from gold surface and experimentally Fourier transformed by a spectrograph and detected by a CCD camera (400×1,340, Andor). To get full 2D absorptive SFG spectra, the first vibrational coherence is numerical Fourier transformed into frequency domain.[39,47,49,50] The HD 1D SFG spectra can be extracted by adding the two phase cycled pump probe spectra together, where the 4th order signals cancel out and only leaves the 2nd order HD 1D SFG spectra. SFG of bare gold was also collected as the reference for phase calibrations. The HD 2D SFG signal is measured at ppppp polarization, where the polarizations of all pulses are set to be p (in plane with the surface normal-incidence beam plane) to the sample, by pairs of waveplates and polarizers, and only p-polarized signal is detected. We note in both our experiment and many other SFG experiments gold surfaces are used as the substrate, which generate the non-resonance SFG signal. The gold SFG signal can interfere with the SFG signal of interests. Therefore, in principle, both experiments are self-heterodyned. The samples are constantly rastered between each scan (~10 min) to avoid sample damaging. To improve signal to noise ratio, multiple scans are averaged for each time step.

2.2 Depolarization ratio measurement from Raman spectroscopy. We compare the experimental Raman depolarization ratio to the calculated results in DFT, in order to determine the accuracy of the calculation and choose the best basis set/functional for the hyperpolarizability calculation. Depolarization experiments were done by collecting polarized Raman spectra of

Re(4,4'-dicyano-2,2'-bipyridine)$(CO)_3Cl$ in DMSO. The spectra were collected with 647.09 nm excitation produced by a mixed argon/krypton gas ion laser. Sample solution was placed in a 1×1 cm fluorescence cuvette and excited through the bottom of the cuvette. Right-angle geometry was used for the excitation and detection of scattered light. Raman scattering was collected and collimated with an F/1.2 camera lens and focused with an achromatic doublet with 300 mm focal length. A dichroic polarizer mounted in a rotation stage and located after the 300 mm lens was used to analyze the parallel and perpendicular Raman scattering. A quartz depolarizer placed before the entrance slit scrambled the polarization to compensate for different instrument responses to parallel/perpendicular light. A 647.1 nm edge filter rejected the excitation line. A single-grating spectrograph with 1200 gr/mm ruled grating was used to disperse the light, and the detector was an open-electrode CCD. Each polarization was collected for a total of 10 minutes. Raman shifts were calibrated from six lines from a neon lamp and three bands of a 50:50 mixture of acetonitrile and toluene having known Raman shifts.

4. RESULTS

4.1 Measuring Orientation Heterogeneity of a Surface Catalyst for CO_2 Reduction. Based on the theory and experiments presented above, we can extract the orientation heterogeneity of the Re(4,4'-dicyano-2,2'-bipyridine)$(CO)_3Cl$ monolayer, self-assembled on a gold slide (Figure 3b), from its HD 2D VSFG spectrum (Figure 3c). [47] The peaks at 2020, 1931, and 1911 cm^{-1} along the diagonal of the HD 2D VSFG spectrum originate from the A'(1), A", and A'(2) modes of $Re(CO)_3$ moiety, respectively (See supporting information), which we can use to extract χ_{eff} and to reveal the orientation heterogeneity of the surface molecules. To extract χ_{eff}, we took diagonal cut of the HD 2D VSFG spectrum (Figure 3c), and extract heterodyne 1D VSFG spectrum directly from HD 2D VSFG raw data.

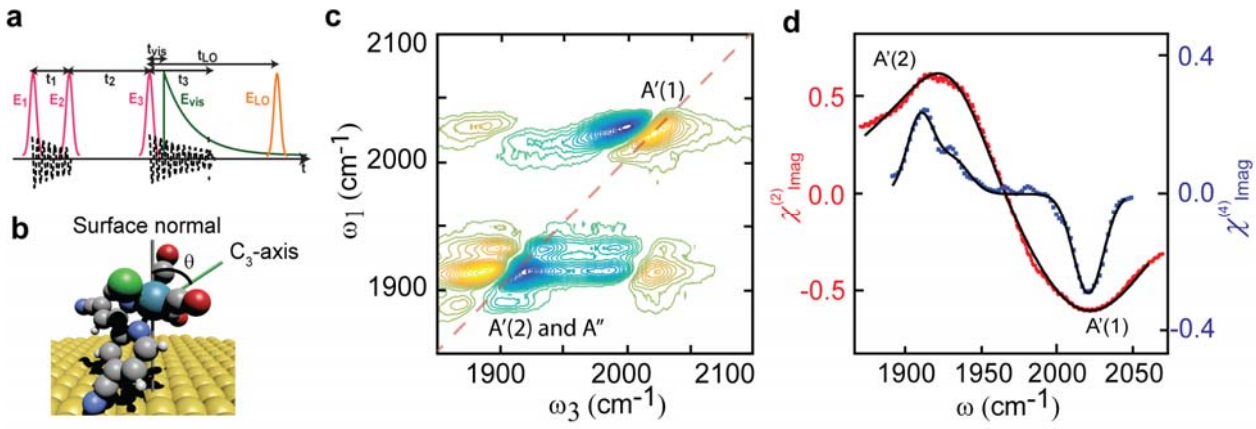

Figure 3. Illustration and results of HD 2D VSFG spectroscopy and the surface catalysis system. (a) HD 2D VSFG pulse sequence. (b) Illustration of Re(4,4'-dicyano-2,2'-bipyridine)$(CO)_3Cl$ monolayer self-assembled on a gold slide. θ_0 is the angle between C_3 axis and surface normal. (c) HD 2D VSFG spectra of the Re complex in the carbonyl stretch region. (d) Heterodyne 1D (red dots) and diagonal cut of HD 2D (blue dots) VSFG spectra. The 1D spectrum has been significantly broadened by surface inhomogeneity. Solid lines represent theoretical fitting.

We determined the χ_{eff} ratios of two vibrational modes by fitting the A'(1) and A'(2) peaks in both the heterodyne 1D VSFG spectrum and the diagonal cut of the HD 2D VSFG spectrum (Figure 3d). From the fittings, we found $\chi^{(2)}_{eff}[A'(1)]/\chi^{(2)}_{eff}[A'(2)]$=-1.31±0.04 and $\chi^{(4)}_{eff}[A'(1)]/\chi^{(4)}_{eff}[A'(2)]$=-1.3±0.1. Since all beams were held at *p* polarization, and the Fresnel factor on gold is strong in the Z direction, we found $\chi^{(2)}_{eff} \propto \chi^{(2)}_{ZZZ}$ and $\chi^{(4)}_{eff} \propto \chi^{(4)}_{ZZZZZ}$. For the case of Re-complex on gold surface, we derived the equation of $\chi^{(2)}_{ZZZ}$ and $\chi^{(4)}_{ZZZZZ}$. By taking a uniform distribution of the in-plane rotation and twist angles, Eq.2 can be written explicitly as:

For A'(1) mode,

$$\chi^{(2)}_{ZZZ}[A'(1)] = N\left[\left(\frac{\beta^{(2)}_{xxz}+\beta^{(2)}_{yyz}}{2}\right)\langle\cos\theta\rangle + \left(\beta^{(2)}_{zzz} - \frac{\beta^{(2)}_{xxz}+\beta^{(2)}_{yyz}}{2}\right)\langle\cos^3\theta\rangle\right]$$
$$\chi^{(4)}_{ZZZZZ}[A'(1)] = N\left[\left(\frac{\beta^{(4)}_{xxzzz}+\beta^{(4)}_{yyzzz}}{2}\right)\langle\cos^3\theta\rangle + \left(\beta^{(4)}_{zzzzz} - \frac{\beta^{(4)}_{xxzzz}+\beta^{(4)}_{yyzzz}}{2}\right)\langle\cos^5\theta\rangle\right] \quad (5)$$

For A'(2) mode,

$$\chi^{(2)}_{ZZZ}[A'(2)] = N\left[\left(\beta^{(2)}_{xzx}\right)\langle\cos\theta\rangle + \left(-\beta^{(2)}_{xzx}\right)\langle\cos^3\theta\rangle\right]$$
$$\chi^{(4)}_{ZZZZZ}[A'(2)] = N\left[\left(\frac{3\beta^{(4)}_{xzxxx}}{4}\right)\langle\cos\theta\rangle + \left(-\frac{3\beta^{(4)}_{xzxxx}}{2}\right)\langle\cos^3\theta\rangle + \left(\frac{3\beta^{(4)}_{xzxxx}}{4}\right)\langle\cos^5\theta\rangle\right] \quad (6)$$

By substituting Eq. 5 and 6 into Eq. 3 and using the numerical value of hyperpolarizabilities calculated by density functional theory (DFT) (B3LYP/LANL2TZ basis set),[45] we derived the numerical relationships between $\chi^{(2)}_{ZZZ,1}/\chi^{(2)}_{ZZZ,2}$, $\chi^{(4)}_{ZZZZZ,1}/\chi^{(4)}_{ZZZZZ,2}$, and D_1, D_2. We found that D_1=0.364±0.008 and D_2=0.14±0.02.

Next, we used the measured D_1 and D_2 to extract all the qualified (θ_0, σ) pairs from the D_1 and D_2 surfaces. With D_1=0.364 and D_2=0.14, we drew two planes that were parallel to the θ_0-σ plane at D'=0.364 and D''=0.14 to intersect the D_1 and D_2 surfaces (Figure 4a and 4b), respectively. The projections of intersecting lines on the θ_0-σ plane represent the qualified (θ_0, σ) pairs that have D_1=D' and D_2=D'' (Figure 4c), and the results agree with our previous statement that there are many combinations of (θ_0, σ) pairs to match a single D_1 value. However, there is only one intersection point (θ_0=53°, σ=5°) between the intersecting lines of D_1 and D_2 that represents the unique (θ_0, σ) pair that satisfies both D_1=D' and D_2=D''.

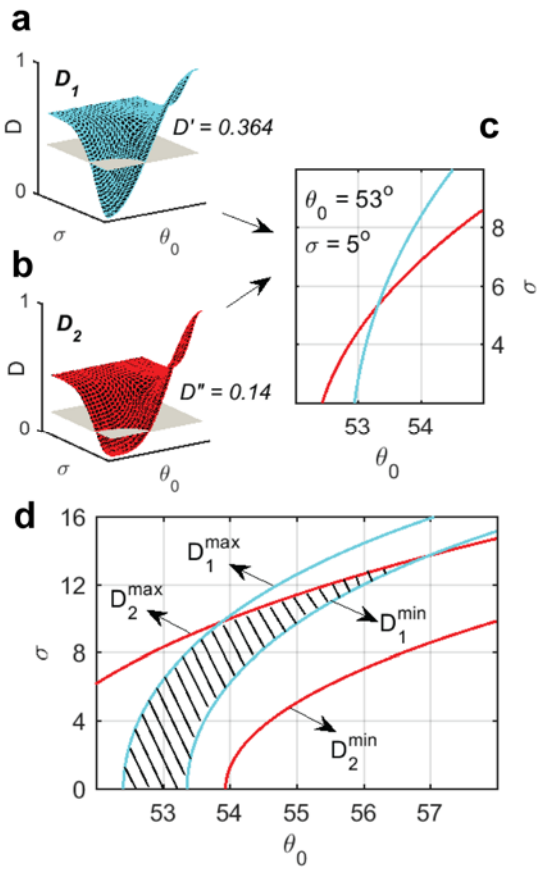

Figure 4. Determination of the unique (θ_0, σ) pair for D_1=0.364 and D_2=0.14. Two planes that are parallel to the θ_0-σ plane are inserted at D'=0.364 in D_1 surface (a) and at D''=0.14 in D_2 surface (b). The projections of both intersecting lines on the θ_0-σ plane are plotted in (c), and the intersection point (θ_0=53°, σ=5°) represents the unique (θ_0, σ) pair. The region of qualified (θ_0, σ) pairs for D_1=0.364±0.008 and D_2=0.14±0.02 is marked in (d).

When taking into account the uncertainty of measured D_1 and D_2, the projected intersecting lines of D_1 and D_2 become stripes on the θ_0-σ plane. Thus the unique intersection point turns into an intersection region, shown as the shaded area in Figure 4d. As a result, θ_0 was found to be in the region of 52~57°, while the range of σ was different for each θ_0 value. The maximum uncertainty of σ is ±4°, when θ_0 is about 53.4°. This result of θ_0=53°, σ=5° suggests that the Re-

complex forms a well-ordered layer. In this case, if assuming a narrow orientational distribution, the mean tilt angle is calculated to be 53°, same as what is determined by our new method, but the orientational distribution information is missing. Most recently, the Lian, Batista and Kubiak research groups studied the orientation of the same molecule self-assembled on a gold surface using a combination of 1D VSFG and DFT simulation, and the angle between the plane of the bi-pyridine ligand and surface normal was found to be 63°.[34] However, no information about orientation heterogeneity was reported.

The well-ordered monolayer experimentally revealed by our work indicates that there is one energetic favorable orientation for all the Re-complex on the gold surface. Because HD 2D VSFG measures a large ensemble average of interfacial molecules, under the ergodic condition, we can conclude that the Re-complexes undergo very small orientation fluctuations over time and are relatively rigid. This could be originated from that the Re-complexes use very short CN groups as the anchoring moieties. Short anchoring groups are often used to increase charge transfer rate, by reducing the electrode-catalysts distance, but they could lead to little flexibility for the catalysts to sample various orientations, as observed from our measurement. It is important for catalysts to be flexible to accommodate different conformations to facilitate reactions.[51] Thus, an optimized anchoring group selection could exist to balance the charge transfer rate, and the flexibility of catalysts. Our work shows the potential of using HD 2D SFG to assess the flexibility of the surface catalysts.

5. DISCUSSION

We note that although the orientational distribution of the Re-catalysts studied here is narrow and the mean tilt angle measured using HD 2D VSFG is essentially the same as the result from

heterodyne 1D VSFG when a narrow distribution is assumed, we are able to experimentally determined that the Re-catalysts form a well-ordered monolayer on the surface, which is a new capability complementary to 1D VSFG. In addition, we note that the discrepancy of the mean tilt angle determined by using our method and the 1D SFG method can be large. For instance, in a hypothetical scenario, when D_1=0.415 is measured and the narrow distribution is assumed, the calculated mean tilt angle is 50°. However, if, with the same sample, D_2=0.23, then the angle would be 67° with distribution of 27°, which means that the angle determined from the narrow distribution assumption has a systematic error of 25%.

There are three important aspects that are influential to the orientation heterogeneity measurement. First, to properly measure surface molecular orientation heterogeneity, it is important to implement heterodyne detection, rather than homodyne detection. In heterodyne and homodyne detections, the measured 2D VSFG signals can be expressed as:[39]

$$S_{\text{heterodyne}} \approx E_{2DVSFG} * E_{LO} \propto \chi_{eff}^{(4)}$$
$$S_{\text{homodyne}} \approx E_{2DVSFG} * E_{1DVSFG} \propto \chi_{eff}^{(4)} * \chi_{eff}^{(2)} \quad (7)$$

When heterodyne detection is used, the measured signal is proportional to $\chi^{(4)}_{eff}$, but when homodyne detection is used, the 1D VSFG signal essentially acts as a local oscillator to heterodyne the 2D VSFG signal. Therefore, the measured signal is proportional to $\chi^{(4)}_{eff} * \chi^{(2)}_{eff}$. As a result, it is difficult to disentangle these two terms and determine the $\chi^{(4)}_{eff}$ ratio from homodyne 2D VSFG.

Second, the values of D_1 and D_2 are the keys to retrieving an accurate (θ_0, σ) pair, which is affected mostly by the signal-to-noise ratio (S/N) in the measurements. This becomes most apparent when σ is relatively large, making both D_1 and D_2 converge and a small change in the D

values could lead to a large difference. In our measurements, the S/N of HD 2D VSFG is about 20, which leads to the same order of magnitude of uncertainty in the spectral fitting mentioned above. Therefore, the experimental noise does not lead to additional uncertainty in the orientation heterogeneity measurements. We note, however, that the relation between D_1 and D_2 is restricted. For instance, a Gaussian distribution requires that $D_1^2 \leq D_2 \leq D_1$. This relation has to be satisfied if a Gaussian distribution is appropriate to describe the orientation heterogeneity of the interfacial molecules; otherwise, other models have to be proposed.

Third, another source of uncertainty comes from the value of hyperpolarizability. Here, we used high level DFT calculations to determine the hyperpolarizability, which is a common approach used in Raman and 1D VSFG spectroscopic studies.[52–57] The accuracy of hyperpolarizability and the resulted (θ_0, σ) pair depends on the choice of basis sets. To evaluate that, we tested basis sets at different levels. The results of hyperpolarizability, Raman depolarization ratio, and corresponding (θ_0, σ) pair is summarized in Table 1. We found the calculated hyperpolarizability converges to a level where the variation of hyperpolarizabilities from different basis sets does not make significant changes to the (θ_0, σ) pair. Another alternative for determining hyperpolarizability is to derive it from the experimental Raman depolarization ratio.[17] However, this method is limited to symmetric vibrational modes with perfect C_{3v} or C_{∞} symmetry. Since the vibrational modes of Re-complex studied here do not have a perfect C_{3v} symmetry, the Raman depolarization approach cannot be directly applied for our study. Nevertheless, a comparison between the experimental measured and the DFT calculated depolarization ratios could indicate the accuracy of the hyperpolarizability calculation. In our work, we found that among all functional/basis set combinations tried in this report, the B3LYP/LanL2TZ functional/basis set calculates the depolarization ratio of the A'(1) and A'(2)

modes to be 0.34 and 0.50, respectively, which matches with the experimental measured ratios : 0.44 and 0.55, best. (Table 1) Therefore, we chose to report the orientation heterogeneity determined from B3LYP/LanL2TZ as our best result. Further investigations of determining hyperpolarizabilities of complex molecules that are lack of rigorous symmetries is important, in order to accurately determine molecular heterogeneity, but it is out of the scope of this initial report.

Table 1. D_1, D_2, θ_0 and σ Determined Using Different Functionals and Basis Sets.

	Experimental value	**B3LYP/ LanL2TZ**	B3LYP/ Def2QZVP	B3LYP/ Def2TZVP	M06L/ LanL2TZ	M06L/ Def2QZVP	M06L/ Def2TZVP
$\rho_{A'(1)}$*	**0.44**	**0.35**	0.32	0.33	0.33	0.30	0.31
$\rho_{A'(2)}$*	**0.55**	**0.50**	0.49	0.50	0.51	0.51	0.51
D_1	/	**0.364**	0.335	0.337	0.336	0.331	0.331
D_2	/	**0.14**	0.13	0.13	0.14	0.12	0.13
θ_0	/	**53**˚	56˚	56˚	58˚	56˚	57˚
σ	/	**5**˚	9˚	9˚	12˚	7˚	10˚

*Depolarization ratio.

6. CONCLUSION

The method in this work can be applied broadly to determine the orientation heterogeneity of interfacial molecules in systems consisting of water, solid state materials and biological molecules, many of which have been investigated by HD 2D VSFG spectroscopy.[40–43,58–61] Therefore, the orientation analysis presented here can be directly applied to these spectral regimes. In addition, since only the diagonal cuts of HD 2D VSFG are analyzed to obtain the orientation heterogeneity, in principle, the same method can be applied to IR pump-SFG probe

experiments[38] when there is no coupling between vibrational modes. This extension enables the orientation heterogeneity measurement by a more established technique than HD 2D VSFG.

In summary, we demonstrate that the orientation heterogeneity of molecules at interfaces can be determined using HD 2D VSFG. In particular, we studied the monolayer of Re(4,4'-dicyano-2,2'-bipyridine)$(CO)_3Cl$ on a gold electrode and found that it forms a fairly ordered structure, which has implications to the surface structure-function relationships. This new advancement solves the long-standing "magic angle" challenge in 1D VSFG spectroscopy. With the growing popularity of HD 2D VSFG spectroscopy in the surface science community,[39–44,47,49,58–63] this new method will contribute significantly in determining the molecular conformations at interfaces.

ASSOCIATED CONTENT

Supporting Information. Illustration of the vibrational modes investigated in this work, brief description of the Euler transformation between laboratory and molecular frames, DFT calculations of the transition dipole moment and polarizability tensor elements, details and results of spectral fitting, description of the modified Gaussian distribution, and description of Raman depolarization ratio measurements. This material is available free of charge via the Internet at http://pubs.acs.org.

AUTHOR INFORMATION

Corresponding Author

Email: w2xiong@ucsd.edu

Author Contributions

†These authors contributed equally.

Notes

The authors declare no competing financial interest.

ACKNOWLEDGMENT

We thank Megan A. Stone and Prof. Michael J. Tauber performing the Raman depolarization measurements of the Re-complex, and for helpful discussions about related topics. We acknowledge M. L. Clark and Prof. C. P. Kubiak for providing the surface catalyst sample. We thank M. Riera, P. Bajaj and Prof. F. Paesani for helping us set up the DFT calculation. This project is supported by The Defense Advanced Research Projects Agency (government grant number D15AP000107).

REFERENCES

(1) Brandt, K.; Chiu, M. E.; Watson, D. J.; Tikhov, M. S.; Lambert, R. M. Chemoselective Catalytic Hydrogenation of Acrolein on Ag(111): Effect of Molecular Orientation on Reaction Selectivity. *J. Am. Chem. Soc.* **2009**, *131*, 17286–17290.

(2) McMillan, D. G. G.; Marritt, S. J.; Kemp, G. L.; Gordon-Brown, P.; Butt, J. N.; Jeuken, L. J. C. The Impact of Enzyme Orientation and Electrode Topology on the Catalytic Activity of Adsorbed Redox Enzymes. *Electrochim. Acta* **2013**, *110*, 79–85.

(3) Barbey, R.; Lavanant, L.; Paripovic, D.; Schuwer, N.; Sugnaux, C.; Tugulu, S.; Klok, H.-A. Polymer Brushes via Surface-Initiated Controlled Radical Polymerization: Synthesis, Characterization, Properties, and Applications. *Chem. Rev.* **2009**, *109*, 5437–5527.

(4) Jailaubekov, A. E.; Willard, A. P.; Tritsch, J. R.; Chan, W.-L.; Sai, N.; Gearba, R.; Kaake, L. G.; Williams, K. J.; Leung, K.; Rossky, P. J.; et al. Hot Charge-Transfer Excitons Set the Time Limit for Charge Separation at Donor/Acceptor Interfaces in Organic Photovoltaics. *Nat. Mater.* **2013**, *12*, 66–73.

(5) Wu, G.; Lee, K. Y. C. Effects of Poloxamer 188 on Phospholipid Monolayer Morphology: An Atomic Force Microscopy Study. *Langmuir* **2009**, *25*, 2133–2139.

(6) Lam, K. L. H.; Ishitsuka, Y.; Cheng, Y.; Chien, K.; Waring, A. J.; Lehrer, R. I.; Lee, K. Y. C. Mechanism of Supported Membrane Disruption by Antimicrobial Peptide Protegrin-1. *J. Phys. Chem. B* **2006**, *110* , 21282–21286.

(7) Cracknell, J. A.; Vincent, K. A.; Armstrong, F. A. Enzymes as Working or Inspirational Electrocatalysts for Fuel Cells and Electrolysis. *Chem. Rev*. 2008, 2439–2461.

(8) Shen, Y. R. Surface Properties Probed by Second-Harmonic and Sum-Frequency Generation. *Nature* **1989**, *337*, 519–525.

(9) Eisenthal, K. B. Liquid Interfaces Probed by Second-Harmonic and Sum-Frequency Spectroscopy. *Chem. Rev.* **1996**, *96*, 1343–1360.

(10) Wang, H.-F.; Velarde, L.; Gan, W.; Fu, L. Quantitative Sum-Frequency Generation Vibrational Spectroscopy of Molecular Surfaces and Interfaces: Lineshape, Polarization, and Orientation. *Annu. Rev. Phys. Chem.* **2015**, *66*, 189–216.

(11) Yan, E. C. Y.; Wang, Z.; Fu, L. Proteins at Interfaces Probed by Chiral Vibrational Sum Frequency Generation Spectroscopy. *J. Phys. Chem. B* **2015**, *119*, 2769–2785.

(12) Li, Z.; Weeraman, C. N.; Gibbs-Davis, J. M. Following the Azide-Alkyne Cycloaddition at the Silica/Solvent Interface with Sum Frequency Generation. *ChemPhysChem* **2014**, *15*, 2247–2251.

(13) Sohrabpour, Z.; Kearns, P. M.; Massari, A. M. Vibrational Sum Frequency Generation Spectroscopy of Fullerene at Dielectric Interfaces. *J. Phys. Chem. C* **2016**, *120*, 1666–1672.

(14) Stiopkin, I. V.; Jayathilake, H. D.; Bordenyuk, A. N.; Benderskii, A. V. Heterodyne-Detected Vibrational Sum Frequency Generation Spectroscopy. *J. Am. Chem. Soc.* **2008**, *130*, 2271–2275.

(15) Hopkins, A. J.; McFearin, C. L.; Richmond, G. L. Investigations of the Solid-Aqueous Interface with Vibrational Sum-Frequency Spectroscopy. *Curr. Opin. Solid State Mater. Sci.* **2005**, *9*, 19–27.

(16) Quast, A. D.; Curtis, A. D.; Horn, B. A.; Goates, S. R.; Patterson, J. E. Role of Nonresonant Sum-Frequency Generation in the Investigation of Model Liquid Chromatography Systems. *Anal. Chem.* **2012**, *84*, 1862–1870.

(17) Wang, H.-F.; Gan, W.; Lu, R.; Rao, Y.; Wu, B.-H. Quantitative Spectral and Orientational Analysis in Surface Sum Frequency Generation Vibrational Spectroscopy (SFG-VS). *Int. Rev. Phys. Chem.* **2005**, *24*, 191–256.

(18) Roy, S.; Covert, P. a; FitzGerald, W. R.; Hore, D. K. Biomolecular Structure at Solid-Liquid Interfaces as Revealed by Nonlinear Optical Spectroscopy. *Chem. Rev.* **2014**, *114*, 8388–8415.

(19) Li, Z.; Weeraman, C. N.; Azam, M. S.; Osman, E.; Gibbs-Davis, J. M. The Thermal Reorganization of DNA Immobilized at the Silica/Buffer Interface: A Vibrational Sum Frequency Generation Investigation. *Phys. Chem. Chem. Phys.* **2015**, *17*, 12452–12457.

(20) Zhuang, X.; Miranda, P.; Kim, D.; Shen, Y. Mapping Molecular Orientation and Conformation at Interfaces by Surface Nonlinear Optics. *Phys. Rev. B* **1999**, *59*, 12632–12640.

(21) Simpson, G.; Westerbuhr, S.; Rowlen, K. Molecular Orientation and Angular Distribution Probed by Angle-Resolved Absorbance and Second Harmonic Generation. *Anal. Chem.* **2000**, *72*, 887–898.

(22) Simpson, G. J.; Rowlen, K. L. An SHG Magic Angle: Dependence of Second Harmonic Generation Orientation Measurements on the Width of the Orientation Distribution. *J. Am. Chem. Soc.* **1999**, *121*, 2635–2636.

(23) Zhu, H.; Dhinojwala, A. Thermal Behavior of Long-Chain Alcohols on Sapphire Substrate. *Langmuir* **2015**, *31*, 6306–6313.

(24) Chen, X.; Minofar, B.; Jungwirth, P.; Allen, H. C. Interfacial Molecular Organization at Aqueous Solution Surfaces of Atmospherically Relevant Dimethyl Sulfoxide and Methanesulfonic Acid Using Sum Frequency Spectroscopy and Molecular Dynamics Simulation. *J. Phys. Chem. B* **2010**, *114*, 15546–15553.

(25) Li, Z.; Weeraman, C. N.; Gibbs-Davis, J. M. Ketone Binding at Amino and Ureido Monolayer/Solvent Interfaces Studied by Nonlinear Optical Techniques. *J. Phys. Chem. C* **2014**, *118*, 28662–28670.

(26) Yamaguchi, S.; Hosoi, H.; Yamashita, M.; Sen, P.; Tahara, T. Physisorption Gives Narrower Orientational Distribution than Chemisorption on a Glass Surface: A Polarization-Sensitive Linear and Nonlinear Optical Study. *J. Phys. Chem. Lett.* **2010**, *1*, 2662–2665.

(27) Kundu, A.; Watanabe, H.; Yamaguchi, S.; Tahara, T. Agreement between Experimentally and Theoretically Estimated Orientational Distributions of Solutes at the Air/Water Interface. *J. Phys. Chem. C* **2013**, *117*, 8887−8891.

(28) Bos, M. A.; Kleijn, J. M. Determination of the Orientation Distribution of Adsorbed Fluorophores Using TIRF. I. Theory. *Biophys. J.* **1995**, *68*, 2566–2572.

(29) Edmiston, P. L.; Lee, J. E.; Cheng, S.-S.; Saavedra, S. S. Molecular Orientation Distributions in Protein Films. 1. Cytochrome C Adsorbed to Substrates of Variable Surface Chemistry. *J. Am. Chem. Soc.* **1997**, *119*, 560–570.

(30) Tronin, A.; Strzalka, J.; Chen, X.; Dutton, P. L.; Blasie, J. K. Determination of the Porphyrin Orientation Distribution in Langmuir Monolayers by Polarized Epifluorescence. *Langmuir* **2000**, *16*, 9878–9886.

(31) Runge, A. F.; Saavedra, S. S.; Mendes, S. B. Combination of Polarized TIRF and ATR Spectroscopies for Determination of the Second and Fourth Order Parameters of Molecular Orientation in Thin Films and Construction of an Orientation Distribution Based on the Maximum Entropy Method. *J. Phys. Chem. B* **2006**, *110*, 6721–6731.

(32) Rao, Y.; Hong, S.-Y.; Turro, N. J.; Eisenthal, K. B. Molecular Orientational Distribution at Interfaces Using Second Harmonic Generation. *J. Phys. Chem. C* **2011**, *115*, 11678–11683.

(33) Rao, Y.; Tao, Y.; Wang, H.-F. Quantitative Analysis of Orientational Order in the Molecular Monolayer by Surface Second Harmonic Generation. *J. Chem. Phys.* **2003**, *119*, 5226–5236.

(34) Clark, M. L.; Rudshteyn, B.; Ge, A.; Chabolla, S. A.; Machan, C. W.; Psciuk, B. T.; Song, J.; Canzi, G.; Lian, T.; Batista, V. S.; et al. Orientation of Cyano-Substituted Bipyridine Re(I) Fac-Tricarbonyl Electrocatalysts Bound to Conducting Au Surfaces. *J. Phys. Chem. C* **2016**, *120*, 1657–1665.

(35) Rosenfeld, D. E.; Gengeliczki, Z.; Smith, B. J.; Stack, T. D. P.; Fayer, M. D. Structural Dynamics of a Catalytic Monolayer Probed by Ultrafast 2D IR Vibrational Echoes. *Science.* **2011**, *334*, 634–639.

(36) Yan, C.; Yuan, R.; Pfalzgraff, W. C.; Nishida, J.; Wang, L.; Markland, T. E.; Fayer, M. D. Unraveling the Dynamics and Structure of Functionalized Self-Assembled Monolayers on Gold Using 2D IR Spectroscopy and MD Simulations. *Proc. Natl. Acad. Sci. U. S. A* **2016**, *113*, 4929–4934.

(37) Xiong, W.; Laaser, J. E.; Paoprasert, P.; Franking, R. A.; Hamers, R. J.; Gopalan, P.; Zanni, M. T. Transient 2D IR Spectroscopy of Charge Injection in Dye-Sensitized Nanocrystalline Thin Films. *J. Am. Chem. Soc.* **2009**, *131*, 18040–18041.

(38) Anfuso, C. L.; Ricks, A. M.; Rodríguez-Cordoba, W.; Lian, T. Ultrafast Vibrational Relaxation Dynamics of a Rhenium Bipyridyl CO_2-Reduction Catalyst at a Au Electrode Surface Probed by Time-Resolved Vibrational Sum Frequency Generation Spectroscopy. *J. Phys. Chem. C* **2012**, *116*, 26377–26384.

(39) Xiong, W.; Laaser, J. E.; Mehlenbacher, R. D.; Zanni, M. T. Adding a Dimension to the Infrared Spectra of Interfaces Using Heterodyne Detected 2D Sum-Frequency Generation (HD 2D SFG) Spectroscopy. *Proc. Natl. Acad. Sci. U. S. A* **2011**, *108*, 20902–20907.

(40) Inoue, K.; Nihonyanagi, S.; Singh, P. C.; Yamaguchi, S.; Tahara, T. 2D Heterodyne-Detected Sum Frequency Generation Study on the Ultrafast Vibrational Dynamics of H_2O and HOD Water at Charged Interfaces. *J. Chem. Phys.* **2015**, *142*, 212431.

(41) Singh, P. C.; Nihonyanagi, S.; Yamaguchi, S.; Tahara, T. Ultrafast Vibrational Dynamics of Water at a Charged Interface Revealed by Two-Dimensional Heterodyne-Detected Vibrational Sum Frequency Generation. *J. Chem. Phys.* **2012**, *137*, 094706.

(42) Laaser, J. E.; Skoff, D. R.; Ho, J. J.; Joo, Y.; Serrano, A. L.; Steinkruger, J. D.; Gopalan, P.; Gellman, S. H.; Zanni, M. T. Two-Dimensional Sum-Frequency Generation Reveals Structure and Dynamics of a Surface-Bound Peptide. *J. Am. Chem. Soc.* **2014**, *136*, 956–962.

(43) Zhang, Z.; Piatkowski, L.; Bakker, H. J.; Bonn, M. Ultrafast Vibrational Energy Transfer at the Water/Air Interface Revealed by Two-Dimensional Surface Vibrational Spectroscopy. *Nat. Chem.* **2011**, *3*, 888–893.

(44) Laaser, J. E.; Zanni, M. T. Extracting Structural Information from the Polarization Dependence of One- and Two-Dimensional Sum Frequency Generation Spectra. *J. Phys. Chem. A* **2013**, *117*, 5875–5890.

(45) Wu, H.; Zhang, W.-K.; Gan, W.; Cui, Z.-F.; Wang, H.-F. An Empirical Approach to the Bond Additivity Model in Quantitative Interpretation of Sum Frequency Generation Vibrational Spectra. *J. Chem. Phys.* **2006**, *125*, 133203.

(46) Boyd, R. W. *Nonlinear Optics*, 3rd ed.; Academic Press: Burlington, MA, 2008.

(47) Wang, J.; Clark, M. L.; Li, Y.; Kaslan, C. L.; Kubiak, C. P.; Xiong, W. Short-Range Catalyst–Surface Interactions Revealed by Heterodyne Two-Dimensional Sum Frequency Generation Spectroscopy. *J. Phys. Chem. Lett.* **2015**, *6*, 4204–4209.

(48) Yan, S.; Tan, H. S. Phase Cycling Schemes for Two-Dimensional Optical Spectroscopy with a Pump-Probe Beam Geometry. *Chem. Phys.* **2009**, *360*, 110–115.

(49) Li, Y.; Wang, J.; Clark, M. L.; Kubiaka, C. P.; Xiong, W. Characterizing Interstate Vibrational Coherent Dynamics of Surface Adsorbed Catalysts by Fourth-Order 3D SFG Spectroscopy. *Chem. Phys. Lett.* **2016**, *650*, 1–6.

(50) Khalil, M.; Demirdöven, N.; Tokmakoff, A. Obtaining Absorptive Line Shapes in Two-Dimensional Infrared Vibrational Correlation Spectra. *Phys. Rev. Lett.* **2003**, *90*, 047401.

(51) Smieja, J. M.; Benson, E. E.; Kumar, B.; Grice, K. A.; Seu, C. S.; Miller, A. J. M.; Mayer, J. M.; Kubiak, C. P. Kinetic and Structural Studies, Origins of Selectivity, and Interfacial Charge Transfer in the Artificial Photosynthesis of CO. *Proc. Natl. Acad. Sci. U. S. A* **2012**, *109*, 15646–15650.

(52) Chase, H. M.; Psciuk, B. T.; Strick, B. L.; Thomson, R. J.; Batista, V. S.; Geiger, F. M. Beyond Local Group Modes in Vibrational Sum Frequency Generation. *J. Phys. Chem. A* **2015**, *119*, 3407–3414.

(53) Fu, L.; Xiao, D.; Wang, Z.; Batista, V. S.; Yan, E. C. Y. Chiral Sum Frequency Generation for in Situ Probing Proton Exchange in Antiparallel β-Sheets at Interfaces. *J. Am. Chem. Soc.* **2013**, *135*, 3592–3598.

(54) Perry, J. M.; Moad, A. J.; Begue, N. J.; Wampler, R. D.; Simpson, G. J. Electronic and Vibrational Second-Order Nonlinear Optical Properties of Protein Secondary Structural Motifs. *J. Phys. Chem. B* **2005**, *109*, 20009–20026.

(55) Nguyen, K. T.; King, J. T.; Chen, Z. Orientation Determination of Interfacial Beta-Sheet Structures in Situ. *J. Phys. Chem. B* **2010**, *114*, 8291–8300.

(56) Nguyen, K. T.; Le Clair, S. V; Ye, S.; Chen, Z. Orientation Determination of Protein Helical Secondary Structures Using Linear and Nonlinear Vibrational Spectroscopy. *J. Phys. Chem. B* **2009**, *113*, 12169–12180.

(57) Xiao, D.; Fu, L.; Liu, J.; Batista, V. S.; Yan, E. C. Y. Amphiphilic Adsorption of Human Islet Amyloid Polypeptide Aggregates to Lipid/Aqueous Interfaces. *J. Mol. Biol.* **2012**, *421*, 537–547.

(58) Bredenbeck, J.; Ghosh, A.; Nienhuys, H.-K.; Bonn, M. Interface-Specific Ultrafast Two-Dimensional Vibrational Spectroscopy. *Acc. Chem. Res.* **2009**, *42*, 1332–1342.

(59) Singh, P. C.; Nihonyanagi, S.; Yamaguchi, S.; Tahara, T. Communication: Ultrafast Vibrational Dynamics of Hydrogen Bond Network Terminated at the Air/Water Interface: A Two-Dimensional Heterodyne-Detected Vibrational Sum Frequency Generation Study. *J. Chem. Phys.* **2013**, *139*, 161101.

(60) Zhang, Z.; Piatkowski, L.; Bakker, H. J.; Bonn, M. Communication: Interfacial Water Structure Revealed by Ultrafast Two-Dimensional Surface Vibrational Spectroscopy. *J. Chem. Phys.* **2011**, *135*, 021101.

(61) Hsieh, C. S.; Okuno, M.; Hunger, J.; Backus, E. H. G.; Nagata, Y.; Bonn, M. Aqueous Heterogeneity at the Air/Water Interface Revealed by 2D-HD-SFG Spectroscopy. *Angew. Chemie Int. Ed.* **2014**, *53*, 8146–8149.

(62) Ghosh, A.; Ho, J.-J.; Serrano, A. L.; Skoff, D. R.; Zhang, T.; Zanni, M. T. Two-Dimensional Sum-Frequency Generation (2D SFG) Spectroscopy: Summary of Principles and Its Application to Amyloid Fiber Monolayers. *Faraday Discuss.* **2015**, *177*, 493–505.

(63) Ho, J.-J.; Skoff, D. R.; Ghosh, A.; Zanni, M. T. Structural Characterization of Single-Stranded DNA Monolayers Using Two-Dimensional Sum Frequency Generation Spectroscopy. *J. Phys. Chem. B* **2015**, *119*, 10586–10596.

TOC

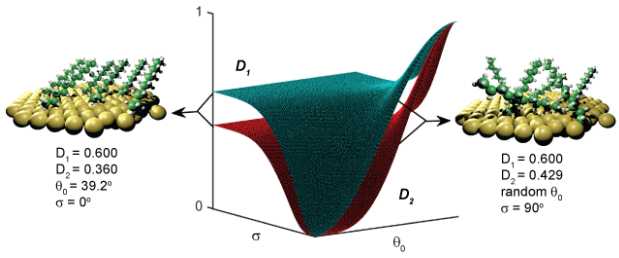
1
0
D1
D2
σ
θ0
D1 = 0.600
D2 = 0.360
θ0 = 39.2°
σ = 0°
D1 = 0.600
D2 = 0.429
random θ0
σ = 90°